Supporting Information

Phase change thermostat for all-day temperature-adaptive thermal regulation

Shuang-Zhu Li, Lu-Ning Wang, Shuai-Peng Wang, Lu Bai, Jie Yang, Wei Yang**

College of Polymer Science and Engineering, Sichuan University, State Key Laboratory of Polymer Materials Engineering, Chengdu 610065, Sichuan, P. R. China

*Corresponding authors.

Tel.: + 86 28 8546 0130; fax: + 86 28 8546 0130.

Email addresses: psejieyang@scu.edu.cn (J. Yang); weiyang@scu.edu.cn (W. Yang)

1. Supplementary Text

1.1 Calculation of solar weighted reflectance and atmospheric window emissivity

According to the measured solar reflectance and infrared emissivity, the solar weighted reflectance $\bar{R}$ is calculated as follows:[S1]

$$\bar{R} = \frac{\int_{\lambda_1}^{\lambda_2} I_{AM1.5}(\lambda) R(\lambda) d\lambda}{\int_{\lambda_1}^{\lambda_2} I_{AM1.5}(\lambda) d(\lambda)} \quad (1)$$

where $I_{AM1.5}$ is AM1.5 global solar irradiance, and $R(\lambda)$ is the spectral reflectance of the surface at wavelength λ.

The average atmospheric window emissivity $\bar{\epsilon}$ is calculated as follows:[S2]

$$\bar{\epsilon} = \frac{\int_{\lambda_1}^{\lambda_2} I_{BB}(T,\lambda) \epsilon(T,\lambda) d\lambda}{\int_{\lambda_1}^{\lambda_2} I_{BB}(T,\lambda) d\lambda} \quad (2)$$

Where $I_{BB}(T,\lambda) = \frac{2hc^2}{\lambda^5} \frac{1}{e^{hc/(\lambda k_B T)} - 1}$ is the spectral radiance emitted by a standard black body at temperature T, h is the Planck's constant, k_B is the Boltzmann constant, and c is the speed of light. $\epsilon(T, \lambda)$ is the spectral emittance of sample.

1.2 Calculation of net cooling power

When an object is exposed to sunlight, its cooling performance is influenced by the solar irradiance, the atmospheric downward thermal radiation, the heat transferred *via* conduction and convection, and the phase change cooling power. Considering all the heat exchange process, the net cooling power P_{net} of the object is calculated by the following equations:[S3-S5]

$$P_{net}(T) = P_{rad}(T) - P_{atm}(T_{amb}) - P_{sun} - P_{cond+conv} + P_{PCMs} \quad (3)$$

where T is the temperature of the object, T_{amb} is the ambient temperature, $P_{rad}(T)$ represents the power radiated out by the object, $P_{atm}(T_{amb})$ is the power generated by incident atmospheric thermal radiation at T_{amb}, P_{sun} is the incident solar irradiation absorbed by the object, $P_{cond+conv}$ is the non-radiative power loss due to the heat convection and conduction, and P_{PCMs} represents the phase change cooling power.

$$P_{rad}(T) = \int d\Omega cos\theta \int_0^\infty d\lambda I_{BB}(T,\lambda)\varepsilon(\lambda,\theta) \quad (4)$$

where Ω is a solid angle, θ denotes the angle between the direction of the solid angle and the normal direction of the surface, $\int d\Omega = 2\pi \int_0^{\pi/2} d\theta sin\theta$ is the angular integral over a hemisphere, and $\varepsilon(\lambda,\theta)$ represents the emissivity of the object at the wavelength (λ) and direction (θ).

$$P_{atm}(T_{amb}) = \int d\Omega cos\theta \int_0^\infty d\lambda I_{BB}(T_{amb},\lambda)\varepsilon(\lambda,\theta)\varepsilon_{atm}(\lambda,\theta) \quad (5)$$

where $\varepsilon_{atm}(\lambda,\theta) = 1 - \tau(\lambda)^{1/cos\theta}$ is the angle-dependent emissivity of the atmosphere, and $\tau(\lambda)$ is the atmospheric transmittance in the zenith direction.

$$P_{sun} = \int_0^\infty d\lambda \varepsilon(\lambda,\theta_{sun}) I_{AM1.5}(\lambda) \quad (6)$$

The solar irradiation is represented by the AM1.5 spectrum $(I_{AM1.5}(\lambda))$. For M10 sample, approximately 94.1% of the input solar irradiance can be reflected, and 5.9% absorption of the solar irradiance will reduce the net cooling power. We assume that the surface of object is facing the sun. Therefore, there is no angular integral for the term P_{sun}, and the corresponding emittance is represented by its value in the zenith direction, *i.e.*, $\theta = 0$.[S6]

$$P_{cond+conv}(T,T_{amb}) = q(T_{amb} - T) \quad (7)$$

where $q = q_{cond} + q_{conv}$ is a combined nonradiative heat coefficient that can be limited from 0 to 12 W m^{-2} K^{-1}.[S7]

$$P_{PCM} = \frac{\Delta H \times m}{t \times A} \quad (8)$$

where A is the surface area of the radiative object, and ΔH is the phase change enthalpy of the object. According to the testing results, we stipulate the enthalpy of M10 is 185 J g^{-1}. The weight (m) of the M10 sample used in the field test is 0.93 g. Term t is the working time of the M10, and the average working time is set as 8 hours.

2. Supplementary Figures and Tables

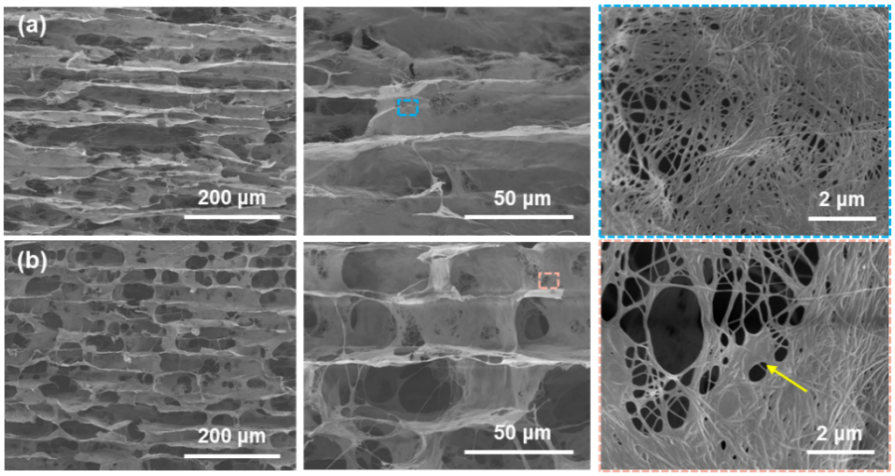

Fig. S1 Cross-sectional SEM images of (a) BC and (b) BC-C aerogels.

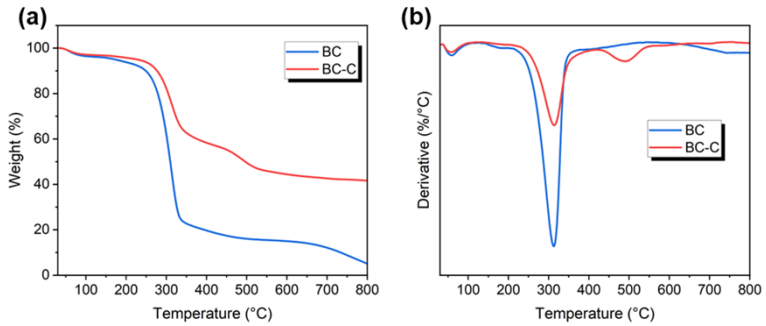

Fig. S2 (a) TGA and (b) DTG curves of BC and BC-C aerogels.

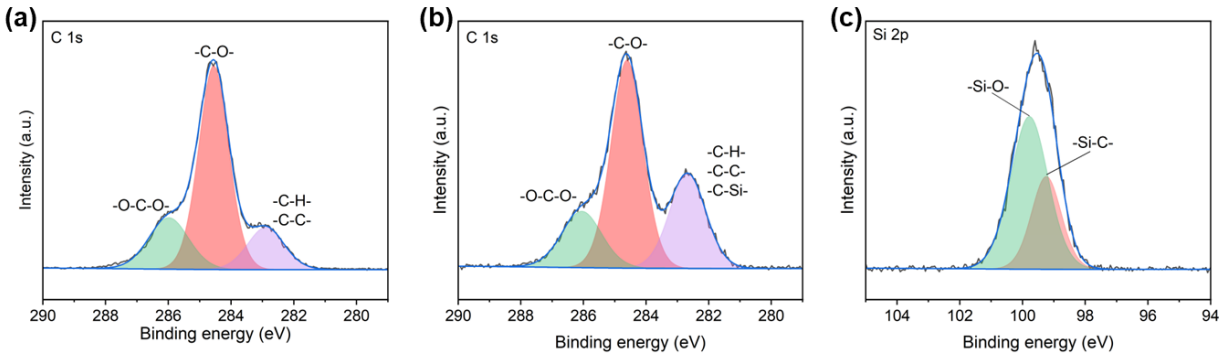

Fig. S3 XPS spectra of BC and BC-C. C 1s XPS spectra of (a) pure BC and (b) BC-C. (c) Si 2p XPS spectrum of BC-C.

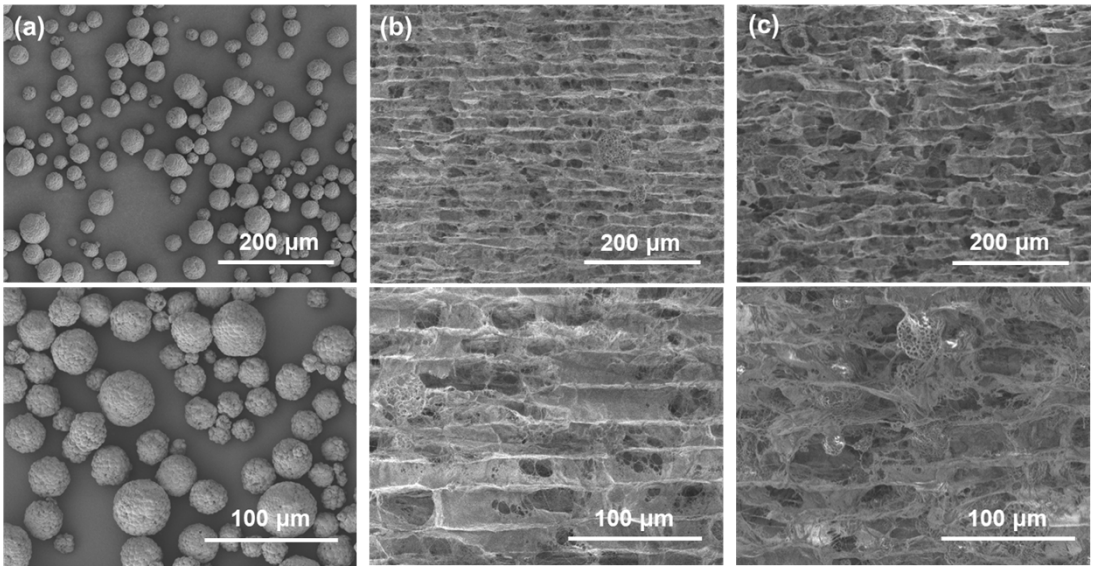

Fig. S4 SEM images of (a) MCPW, (b) M2.5, and (c) M5.

Fig. S5 Digital photo of colored water deposited on the surface of BC aerogel and the water contact angle image of BC aerogel.

Fig. S6 Demonstration of flexibility and elasticity of a phase change thermostat.

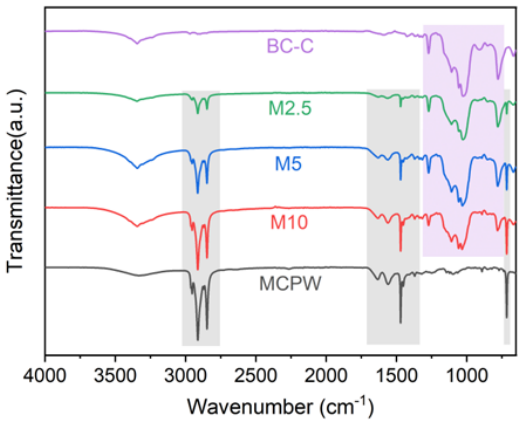

Fig. S7 FT-IR spectra of BC-C, MCPW, and phase change insulation materials.

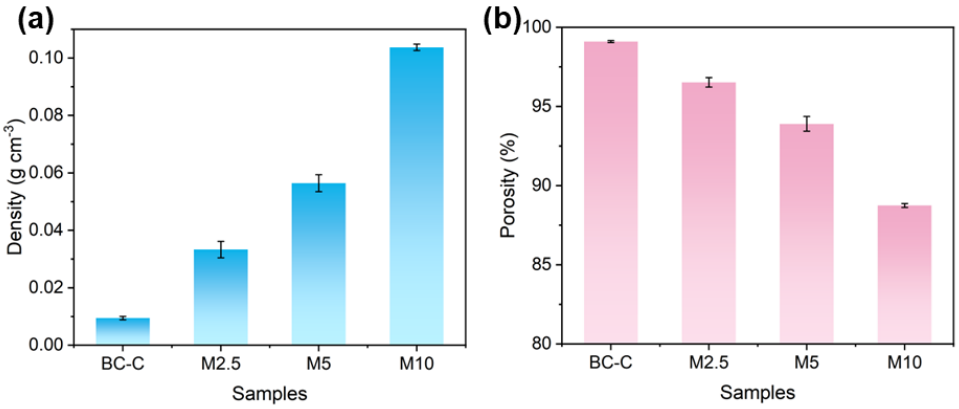

Fig. S8 (a) Density and (b) porosity of BC-C and phase change insulation materials.

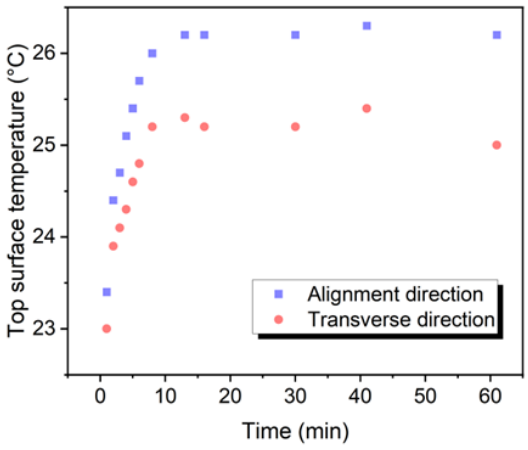

Fig. S9 Evolutions of top surface temperature of M10 along alignment and transverse directions during heating.

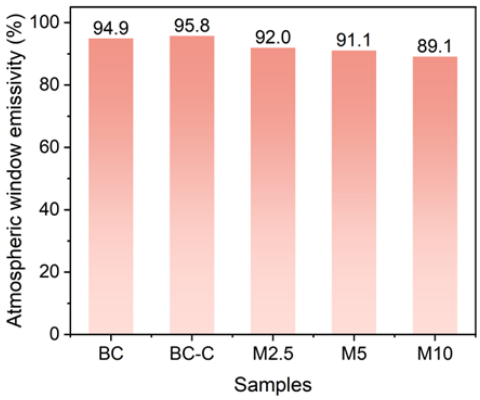

Fig. S10 Atmospheric window emissivity of BC, BC-C, and phase change insulation materials.

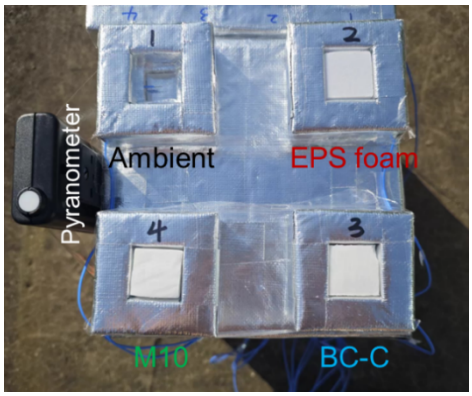

Fig. S11 Photograph showing the experimental device for measuring outdoor thermal management performance.

Fig. S12 Digital photo of large-size M10 prepared by a block-by-block freeze-casting method.

Table S1 DSC heating and cooling characteristics of MCPW and phase change insulation materials.

Samples	T_c (°C)	ΔH_c (J g^{-1})	T_m (°C)	ΔH_m (J g^{-1})
MCPW	19.4	196.3	38.5	**200.4**
M10	18.5	180.5	39.2	**185.0**
M5	19.2	164.5	38.5	**168.3**
M2.5	19.5	140.2	38.4	**143.7**

*T_c, ΔH_c, T_m, and ΔH_m represent crystallization temperature, crystallization enthalpy, melting temperature, and melting enthalpy, respectively.

Table S2 Comparison of cooling performance between M10 in this work and previously reported insulating radiative coolers.

Materials	Thermal conductivity ($mW\ m^{-1}K^{-1}$)	Solar reflectance (%)	Thermal emissivity (%)	Daytime temperature reduction (°C)	Nighttime temperature reduction (°C)	Reference
SiO_2/Wood fiber	/	95.5	> 90.0	~ 6.0	~ 8.0	2021[S8]
Silane/Cellulose nanocrystal (CNC)	29	96.0	92.0	~ 9.2	~ 5.3	2022[S6]
Polyurethane (PU)/Boron nitride nanosheets (BNNS)	16.9	97.0	88.0	~ 13.0	/	2022[S9]
Polyvinyl alcohol (PVA)/ BNNS	23.5	93.8	/	~ 10.0	/	2022[S10]
Cellulose nanofibrils (CNF)/Sodium alginate (SA)	25	88.0	95.0	~ 7.0	/	2023[S11]
poly (vinylidene fluoride) nanocomposites	/	91.8	94.3	~ 8.3	~ 12.0	2023[S12]
Wood pulp cellulose	38.5	92.8	98.2	~ 7.2	/	2023[S13]
PVA/Esterified cellulose	26.2	95.0	97.2	~ 10.2	~ 0.65	2024[S14]
Polyhedral oligomeric silsesquioxane/pre-polymerized vinyl trimethoxy silane	25.5	70.2	99.0	~ 3.7	/	2024[S15]
silica-hybridized cellulose acetate	41	96.0	97.0	~ 9.2	~ 5.3	2024[S16]
SA/Sodium phytate /Thermochromic microcapsules/BN	40	91.8	84.3	~5.6	/	2024[S17]
CNF/CNC/MTMS	28	97.5	93.0	~7.6	/	2024[S18]
Thermoplastic polyurethane (TPU)	/	93.0	96.0	~ 8.6	~ 5.9	2024[S19]
CNF/PVA/ZnO/MOF	/	96.5	94.0	~ 7.5	/	2024[S20]
CNF/SA@LiCl	37.4	97.0	91.0	~ 9.3	/	2024[S21]
BC/MTMS/MCPW	**42.3**	**94.1**	**89.1**	**~ 12.0**	**~ -1.5**	**This Work**

References

S1. Y. Chen, J. Mandal, W. Li, A. Smith-Washington, C.-C. Tsai, W. Huang, S. Shrestha, N. Yu, R. P. S. Han, A. Cao and Y. Yang, *Sci. Adv.*, 2009, **6**, eaaz5413.

S2. J. Song, W. Zhang, Z. Sun, M. Pan, F. Tian, X. Li, M. Ye and X. Deng, *Nat. Commun.*, 2022, **13**, 4805.

S3. M. Yang, H. Zhong, T. Li, B. Wu, Z. Wang and D. Sun, *ACS Nano*, 2023, **17**, 1693-1700.

S4. S. Fan and W. Li, *Nat. Photonics*, 2022, **16**, 182-190.

S5. A. P. Raman, M. A. Anoma, L. Zhu, E. Rephaeli and S. Fan, *Nature*, 2014, **515**, 540-544.

S6. C. Cai, Z. Wei, C. Ding, B. Sun, W. Chen, C. Gerhard, E. Nimerovsky, Y. Fu and K. Zhang, *Nano Lett.*, 2022, **22**, 4106-4114.

S7. T. Wang, Y. Wu, L. Shi, X. Hu, M. Chen and L. Wu, *Nat. Commun.*, 2021, **12**, 365.

S8. Y. Chen, B. Dang, J. Fu, C. Wang, C. Li, Q. Sun and H. Li, *Nano Lett.*, 2021, **21**, 397-404.

S9. K. Y. Chan, X. Shen, J. Yang, K. T. Lin, H. Venkatesan, E. Kim, H. Zhang, J. H. Lee, J. Yu, J. Yang and J. K. Kim, *Nat. Commun.*, 2022, **13**, 5553.

S10. J. Yang, K. Y. Chan, H. Venkatesan, E. Kim, M. H. Adegun, J. H. Lee, X. Shen and J. K. Kim, *Nano-Micro Lett.*, 2022, **14**, 54.

S11. W. Yang, P. Xiao, S. Li, F. Deng, F. Ni, C. Zhang, J. Gu, J. Yang, S.-W. Kuo, F. Geng and T. Chen, *Small*, 2023, **19**, 2302509.

S12. J. Ni, Y. Zhang, Z. Song, P. Zhang, Y. Cao, Y. Yang, W. Wang and J. Wang, *Compos. Part A Appl. Sci. Manuf.*, 2023, **164**, 107311.

S13. S. Zhong, S. Yuan, X. Zhang, J. Zhang, L. Xu, T. Xu, T. Zuo, Y. Cai and L. Yi, *ACS Appl. Mater. Interfaces*, 2023, **15**, 39807-39817.

S14. Y. Bai, X. Jia, Z. Shan, C. Huang, D. Wang, J. Yang, B. Pang and H. Song, *Carbohydr. Polym.*, 2024, **333**, 121951.

S15. H. Ma, M. Fashandi, Z. Ben Rejeb, P. Buahom, J. Zhao, P. Gong, Q. Shi, G. Li and C. B. Park, *J. Mater. Chem. A*, 2024, **12**, 9627-9636.

S16. Y. Liu, X. Bu, R. Liu, M. Feng, Z. Zhang, M. He, J. Huang and Y. Zhou, *Chem. Eng. J.*, 2024, **481**, 148780.

S17. W. Cai, Z. Li, H. Xie, W. Wang, T. Cui, B. Lin, L. Qi, X. Hu, Y. Du, Y. Ming, S. Shi, D. Chen, B. Fei, W. Xing and Y. Hu, *Chem. Eng. J.*, 2024, **483**, 149006.

S18. C. Cai, Y. Chen, C. Ding, Z. Wei and X. Wang, *Mater. Horiz.*, 2024, **11**, 1502-1514.

S19. Y. Lin, C. Qin, Z. Liang, W. Lin, J. Wang and D. Li, *Adv. Opt. Mater.*, 2024, 2401020.

S20. A. Geng, Y. Han, J. Cao and C. Cai, *Int. J. Biol. Macromol.*, 2024, **264**, 130676.

S21. Y. Chen, Y. Sun, F. Cheng, Y. Ji, C. Cai and Y. Fu, *ACS Sustainable Chem. Eng.*, 2024, **12**, 10680-10692.